2011 American Control Conference
on O'Farrell Street, San Francisco, CA, USA
June 29 - July 01, 2011

Sliding Mode Based Integrated Guidance and Autopilot for Chasing UAV with the Concept of Time-Scaled Dynamic Inversion

Takeshi Yamasaki, S. N. Balakrishnan, and Hiroyuki Takano

Abstract— **Integrated guidance and control approaches exploit the synergy between the guidance and the control of a vehicle. This study focuses on the integrated guidance and control(autopilot) design for a chasing UAV against a target aircraft. A second-order sliding structure for desired coupled roll and pull-up motions is proposed as a means to develop an integrated guidance and autopilot scheme. For easier design synthesis, intermediate control variables for partial derivatives of a sliding surface are carefully selected. As a consequence, the sliding surface structure is simple and sufficient to relate the actuator input to the sliding surface. The potential of the proposed method is demonstrated through an aircraft application by comparison of its simulation performance, and the number of tuning parameters with a synthesis technique where the guidance law and the controller are designed independently.**

I. Introduction

UAV (Uninhabited Aerial Vehicles) deployments are expanding rapidly in recent times. UAV operations are, so far, limited in scope of the tasks that they can perform due to payload restrictions. In order to obviate this limitation, schemes with cooperative tasks amongst the UAVs are expected to emerge which could help result in higher payloads and perhaps conduct multi-tasks simultaneously. Automated rendezvous and successive aerial refueling or leader-following capabilities are amongst the most demanding capabilities for the cooperative tasks that might call for the UAV deployments. This paper focuses on the rendezvous with a cooperative aircraft and chasing for aerial refueling and/or following a leader from behind. For this purpose, a system to guide the UAV to a rendezvous point with a desired heading angle constraint is required. The proportional navigation guidance (PNG) has been used for rendezvous and/or missile engagements [1]. PNG with a fixed navigation constant guides the UAV to a collision course (rendezvous course) by keeping the line-of-sight angle constant. The problem with this approach is that the heading angle at the rendezvous is not guaranteed to be a specified value. In order to overcome this problem, a variable navigation constant was proposed to achieve the rendezvous (impact) angle for perfect/imperfect guidance [2, 3]. Ref. [4] applied this theory to the aircraft rendezvous for aerial refueling. It was reported in the literature [4] that when a slight change in the navigation constant is used to avoid a numerical singularity, it led to errors in the rendezvous point and the heading angle and a different controller had to be used when the UAV was close to the tanker. On the other hand, the pure pursuit guidance (PPG) lets the UAV head towards a moving target at any time. The PPG has a tendency to guide the UAV to a tail-chase position against a moving target if the UAV is not on the perfect head on course [5]. Since the perfect head on course rarely occurs, the tail-chase position is guaranteed using the PPG. However, when the UAV comes close to the target, the pure pursuit guidance tends to become sensitive to the target maneuver and therefore, might cause a command divergence problem. In past research, the authors developed a pure pursuit guidance law via a sliding mode approach [6], referred to as a "sliding mode based pure pursuit guidance (SM-PPG)"; the SM-PPG showed robust performance against uncertain target maneuvers. The SM-PPG is still based on the PPG concept using the line-of-sight (LOS) in a three-dimensional representation but is implemented with a sliding mode technique [7]. Galzi and Shtesell [8] applied higher-order sliding modes (HOSM) for UAV formations to calculate the guidance force in a two-dimensional plane. As for a missile application, a sliding mode guidance and autopilot methodology with a zero-effort-miss guidance concept was proposed [9]. It showed better performance than the independent guidance and control design approaches. Sliding mode control for a non minimum phase system was proposed in [10]. Non-minimum phase dynamics, considered as uncertainties. HOSM (for example, Refs.[11, 12, 13]) mitigates the problems related to the sliding mode control (SMC), i.e., HOSM is applicable for arbitrary relative degree systems with smooth control. Shtessel et. al. [12] and Harl et al. [13] applied the HOSM or second order sliding modes (SOSM) for missile interception (with an HOSM observer in [12])against uncertain target maneuvers. In this paper, we develop an integrated guidance technique for an aircraft. Coupled roll and pull-up motions should be taken into account for designing the aircraft autopilot. In this paper, some intermediate control variables and a second order sliding surface are introduced to handle such coupled motion while avoiding the non-minimum phase behavior which occurs in a conventional aircraft. One of the authors introduced second order sliding surfaces for the integrated guidance and control [14], which can drastically reduce the number of the tuning parameters to only two. This study

Takeshi Yamasaki and Hiroyuki Takano are with the Department of Aerospace Engineering, the National Defense Academy of Japan, Kanagawa, 239-8686 JAPAN (e-mail: ymski@nda.ac.jp; htakano0@nda.ac.jp).

S. N. Balakrishnan is with the Department of Mechanical and Aerospace Engineering, Missouri University of Science and Technology, Rolla, MO 65409, USA. (e-mail: bala@mst.edu).

applies the second order sliding surface methodology for the aircraft roll and pull up coupled motions taking account of the aircraft's time-scaled dynamics. This new integrated guidance and control(IGC) design is achieved with the help of the SM-PPG. IGC approaches offer great promise in design since they eliminate the costly (timewise and manpowerwise) iterative guidance and control loops. In this paper, we compare the performance of the developed technique with that of a separate guidance-separate controller design. The rest of the paper is organized as follows: kinematics of the problem to be solved is posed in section II. In section III, the proposed integrated guidance and control scheme via an SMC for a chasing UAV is developed in detail. In section IV, potential of the new approach is demonstrated with representative simulation results. Conclusions are presented in Section V.

II. Problem Statement

Assume that a UAV with the velocity of $\boldsymbol{V}_{UAV}$ pursues a target aircraft as shown in Fig. 1. In order to guide the UAV to pursue the target aircraft, the line of sight (LOS) vector $\boldsymbol{R}$ and the UAV's velocity vector $\boldsymbol{V}_{UAV}$ should head in the same direction. The physics of the problem can then be expressed mathematically as

$$\boldsymbol{V}_{UAV} \times \boldsymbol{R} = \boldsymbol{0} \tag{1}$$

The above equation can be represented in a normalized form as

$$\boldsymbol{S}_o \equiv \frac{\boldsymbol{V}_{UAV} \times \boldsymbol{R}}{V_{UAV} R} \tag{2}$$

where R denotes the norm of the LOS vector, $\boldsymbol{R}$, that is, $R = \|\boldsymbol{R}\|$, and $\boldsymbol{S}_o$ is the basic sliding surface vector in this study. The velocity vector and the LOS vector can be represented with respect to the velocity axes as

$$\boldsymbol{V}_{UAV} = \begin{pmatrix} V_{UAV} & 0 & 0 \end{pmatrix}^T \tag{3}$$

$$\boldsymbol{R} = \begin{pmatrix} x_R & y_R & z_R \end{pmatrix}^T \tag{4}$$

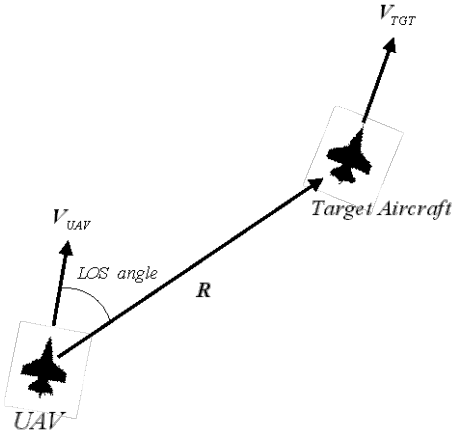

Fig. 1. Position view of the UAV and the target aircraft.

The substitution of these components for Eq. (2) can be reduced to

$$\boldsymbol{S}_o = \begin{pmatrix} 0 & s_1 & s_2 \end{pmatrix}^T \tag{5}$$

where

$$s_1 = -z_R / R \;,\; s_2 = y_R / R \tag{6}$$

The problem is to guide and control the UAV into the target aircraft direction in a way that the vector of Eq. (5) converges to zero vector, or the variables s_1, and s_2 tend to zero.

III. Integrated Guidance and Autopilot

The objective in this study is to reduce the variables, s_1, and s_2 in Eq. (6) with respect *to the velocity axes and not the inertial frame*. Hereafter, the time derivative with respect to the velocity axes, denoted by a prime; $()'$ is referred as a "primed time derivative" in this study. Taking the primed time derivatives of s_1 and s_2 in Eq. (6) yields

$$s_1' = a\dot{\gamma} + b_1 \tag{7}$$

$$s_2' = a\dot{\lambda}\cos\gamma + b_2 \tag{8}$$

where $\dot{\gamma}$ is the flight path angle rate, and $\dot{\lambda}$ is the heading angle rate, and

$$a = -x_R / R$$

$$b_1 = -y_R \dot{\lambda} \tan\gamma / R - V_{T,z} / R + z_R \left\{ x_R \left(V_{T,x} - V_{UAV} \right) + y_R V_{T,y} + z_R V_{T,z} \right\} / R^3$$

$$b_2 = -z_R \dot{\lambda} \tan\gamma / R + V_{T,y} / R - y_R \left\{ x_R \left(V_{T,x} - V_{UAV} \right) + y_R V_{T,y} + z_R V_{T,z} \right\} / R^3$$

The flight path angle, γ, and the heading angle, λ are treated as intermediate control variables. The dynamics of these two variables can be written as (with respect to a point mass model)

$$\dot{\gamma} = \left(L + F_T \sin\alpha \right) \cos\mu / (m V_{UAV}) - g\cos\gamma / V_{UAV} \equiv f_\gamma(\alpha, \mu) \tag{9}$$

$$\dot{\lambda}\cos\gamma = \left(L + F_T \sin\alpha \right) \sin\mu / (m V_{UAV}) \equiv f_\lambda(\alpha, \mu) \tag{10}$$

where m and g, denote the UAV mass and the gravity constant, L and F_T are lift and thrust forces, α and μ are the angle of attack and the bank angle, respectively. It is assumed that there is no sideslip and that the thrust is constant. Equations (9) and (10) imply that the flight path angle and heading angle can be controlled by the angle of attack, α and the bank angle, μ. Equations (7) and (8) can be rearranged using Eqs. (9) and (10) as

$$s_1' = a f_\gamma(\alpha, \mu) + b_1 \tag{11}$$

$$s_2' = a f_\lambda(\alpha, \mu) + b_2 \tag{12}$$

Note that the sideslip motion of the UAV is neglected in the equations expressed in Eqs. (9) and (10) for the dynamics of s_1, and s_2 which is controlled by the angle of attack, α and bank angle, μ. For this purpose, an additional sliding surface

is defined using the side slip angle, β, as,

$$s_3 = \beta \tag{13}$$

Sideslip angle, β, angle of attack, α and bank angle, μ form the second intermediate control variables. Since the sideslip angle, should be always attenuated regardless of any frame, the usual time derivative can be taken for s_3 as

$$\dot{s}_3 = \dot{\beta} \tag{14}$$

Using the definition in Eqs. (9) and (10) leads to the primed time derivatives of s_1' and s_2' as

$$s_1'' = a\left(c_{11}\dot{\alpha} + c_{12}\dot{\mu}\right) + d_{2,1} \tag{15}$$

$$s_2'' = a\left(c_{21}\dot{\alpha} + c_{22}\dot{\mu}\right) + d_{2,2} \tag{16}$$

where

$$c_{11} = \left(q_D S_W C_{L\alpha} + F_T \cos\alpha\right)\cos\mu/(mV_{UAV}) \cong \frac{\partial f_\gamma(\alpha,\mu)}{\partial\alpha}$$

$$c_{12} = -\left(L + F_T \sin\alpha\right)\sin\mu/(mV_{UAV}) \cong \frac{\partial f_\gamma(\alpha,\mu)}{\partial\mu}$$

$$c_{21} = \left(q_D S_W C_{L\alpha} + F_T \cos\alpha\right)\sin\mu/(mV_{UAV}) \cong \frac{\partial f_\lambda(\alpha,\mu)}{\partial\alpha}$$

$$c_{22} = \left(L + F_T \sin\alpha\right)\cos\mu/(mV_{UAV}) \cong \frac{\partial f_\lambda(\alpha,\mu)}{\partial\mu}$$

$$d_{2,1} \cong a' f_\gamma(\alpha,\mu) + b_1' \cong 0$$

$$d_{2,2} \cong a' f_\lambda(\alpha,\mu) + b_2' \cong 0$$

In the last two equations, a, b_1, and b_2 are treated as constant since changes in those value are negligible compared to those of the fast time-scale variables, α and μ. The symbols q_D, S_W, and $C_{L\alpha}$ are the dynamic pressure, the wing area, and the lift curve slope of the UAV, respectively. Define a new sliding surface vector as

$$\boldsymbol{\sigma} = \begin{pmatrix} s_1'' + 2\zeta\omega_n s_1' + \omega_n^2 s_1 \\ s_2'' + 2\zeta\omega_n s_2' + \omega_n^2 s_2 \\ \dot{s}_3 + 2\zeta\omega_n s_3 \end{pmatrix} \equiv \begin{pmatrix} \sigma_1 \\ \sigma_2 \\ \sigma_3 \end{pmatrix} \tag{17}$$

where ζ, the damping coefficient is set at a value of $\sqrt{2}/2$; ω_n, the natural frequency for the sliding surface is treated as a design parameter. It is interesting to note that the highest order term in each component in Eq. (17) corresponds to the fast states (body rates), and the second highest-order terms correspond to the slow states (angle of attack, sideslip angle, and bank angle), and the variables, s_1, and s_2 correspond to the flight path angles(flight path angle and heading angle). If the dynamics reach the sliding manifolds of Eq. (17), the $\boldsymbol{\sigma}$-dynamics converges to zero with time. During this time, the rotation rates, and the attitude and flight path angles will gradually converge, with the time-histories dictated by the design parameter, ω_n. Substitution of Eqs. (15) and (16) in Eq. (17) yields

$$\boldsymbol{\sigma} = G_s \begin{pmatrix} \dot{\alpha} \\ \dot{\beta} \\ \dot{\mu} \end{pmatrix} + \boldsymbol{g}_s \tag{18}$$

where

$$G_s = \begin{bmatrix} ac_{11} & 0 & ac_{12} \\ ac_{21} & 0 & ac_{22} \\ 0 & 1 & 0 \end{bmatrix}$$

$$\boldsymbol{g}_s = \begin{pmatrix} 2\zeta\omega_n s_1' + \omega_n^2 s_1 \\ 2\zeta\omega_n s_2' + \omega_n^2 s_2 \\ 2\zeta\omega_n \beta \end{pmatrix}$$

Note that the dynamics of the angle of attack, the side slip angle, and the bank angle can be described through their relation to the body rates, $\boldsymbol{\omega} = (p \quad q \quad r)^{\mathrm{T}}$, as

$$\left(\dot{\alpha} \quad \dot{\beta} \quad \dot{\mu}\right)^T = B_s\boldsymbol{\omega} + \boldsymbol{d}_s \tag{19}$$

where

$$B_s = \begin{bmatrix} -\cos\alpha\tan\beta & 1 & -\sin\alpha\tan\beta \\ \sin\alpha & 0 & -\cos\alpha \\ \cos\alpha/\cos\beta & 0 & \sin\alpha/\cos\beta \end{bmatrix}$$

$$\boldsymbol{d}_s = \left(d_{s,1} \quad d_{s,2} \quad d_{s,3}\right)^{\mathrm{T}}$$

$$d_{s,1} = (mg\cos\mu\cos\gamma - L - F_T\sin\alpha)/(mV_{UAV}\cos\beta)$$

$$d_{s,2} = (mg\sin\mu\cos\gamma + Y - F_T\cos\alpha\cos\beta)/(mV_{UAV})$$

$$\begin{aligned} d_{s,3} = \{&(-mg\cos\mu\cos\gamma\tan\beta \\ &+ Y\cos\mu\tan\gamma + L(\tan\beta + \sin\mu\tan\gamma) \\ &+ F_T(\sin\alpha\tan\beta - \cos\mu\tan\gamma\cos\alpha\sin\beta \\ &+ \sin\mu\tan\gamma\sin\alpha)\ \}/(mV_{UAV}) \end{aligned}$$

Equation (18) can be rearranged by using Eq. (19) as

$$\boldsymbol{\sigma} = G_s B_s \begin{pmatrix} p \\ q \\ r \end{pmatrix} + G_s\boldsymbol{d}_s + \boldsymbol{g}_s \tag{20}$$

Since the body rate, $\boldsymbol{\omega} = (p \quad q \quad r)^{\mathrm{T}}$ in Eq. (20) can drive the new sliding vector, $\boldsymbol{\sigma}$ to a zero vector, $\boldsymbol{\omega}$ is referred as the third intermediate control variable. Taking the time derivative of Eq. (20) provides

$$\dot{\boldsymbol{\sigma}} = G_s B_s \begin{pmatrix} \dot{p} \\ \dot{q} \\ \dot{r} \end{pmatrix} + \boldsymbol{d}_4 \tag{21}$$

where

$$\boldsymbol{d}_4 = \left[\frac{d}{dt}\left[G_s B_s\right]\right]\begin{pmatrix} p \\ q \\ r \end{pmatrix} + \dot{\boldsymbol{g}}_s + \frac{d}{dt}\left(G_s\boldsymbol{d}_s\right) = \dot{\boldsymbol{g}}_s + \boldsymbol{d}_5$$

$$\boldsymbol{d}_5 = \left[\frac{d}{dt}\left[G_s B_s\right]\right]\begin{pmatrix} p \\ q \\ r \end{pmatrix} + \frac{d}{dt}\left(G_s\boldsymbol{d}_s\right)$$

The term, $\boldsymbol{d}_5$ is treated as a bounded disturbance vector. Equations of the rotational motion for the rigid body can be

expressed as

$$\dot{\boldsymbol{\omega}} = B_f \boldsymbol{u} + \boldsymbol{d}_f \tag{22}$$

where

$$B_f \cong I_m^{-1} q_D S_W diag(bC_{l,\delta a}, \bar{c}C_{m,\delta e}, bC_{n,\delta r})$$

$$I_m = \begin{bmatrix} I_x & 0 & -I_{xz} \\ 0 & I_y & 0 \\ -I_{xz} & 0 & I_z \end{bmatrix}$$

$$\boldsymbol{d}_f = I_m^{-1} (d_{f,1} \quad d_{f,2} \quad d_{f,3})^T$$

$$d_{f1} \cong (I_y - I_z)qr + I_{xz}pq + q_D S_W bC_{lp} p$$

$$d_{f2} \cong (I_z - I_x)pr + I_{xz}(r^2 - p^2) + q_D S_W \bar{c}(C_{m0} + C_{m\alpha}\alpha + C_{mq}q)$$

$$d_{f3} \cong (I_x - I_y)pq - I_{xz}qr + q_D S_W b(C_{n\beta}\beta + C_{nr}r)$$

The control $\boldsymbol{u} = (\delta_a \quad \delta_e \quad \delta_r)^{\mathrm{T}}$ is a 3-dimensional control surface vector (aileron, elevator, and rudder deflections). $C_{(\,)}$ indicates the aerodynamic moment coefficients. I_x, I_y, I_z are the moments of inertia along the body axes and p, q, and r are the body rates. I_m, b, and $\bar{c}$ denote the inertial matrix, the wing span, and the mean aerodynamic chord, respectively. Finally, substituting Eq. (22) into Eq. (21) provides

$$\dot{\boldsymbol{\sigma}} = G_s B_s B_f \boldsymbol{u} + G_s B_s \boldsymbol{d}_f + \boldsymbol{g}_s + \boldsymbol{d}_5 \tag{23}$$

The SOSM [12] may be applied to the sliding surface structure of Eq. (17) for a finite time convergence. However, we use a simple first order sliding mode approach. For this purpose, a Lyapunov function for the SMIGC can be chosen as

$$V_L = \frac{1}{2}\boldsymbol{\sigma}^T \boldsymbol{\sigma} \tag{24}$$

Taking the time derivative of the Lyapunov function above leads to

$$\begin{aligned} \dot{V}_L &= \boldsymbol{\sigma}^T \dot{\boldsymbol{\sigma}} \\ &= \boldsymbol{\sigma}^T (G_s B_s B_f \boldsymbol{u} + G_s B_s \boldsymbol{d}_f + \boldsymbol{g}_s + \boldsymbol{d}_5) \end{aligned} \tag{25}$$

In order to achieve the sliding surfaces of Eq. (17), the control can be selected such that the above differentiated Lyapunov function is always negative, that is

$$\boldsymbol{u} = -(G_s B_s B_f)^{-1} \left\{ G_s B_s \boldsymbol{d}_f + \boldsymbol{g}_s + diag\left[\mathrm{sgn}(\sigma_i)\right]\boldsymbol{\eta} \right\} \tag{26}$$

where σ_i is the ith element of the vector, $\boldsymbol{\sigma}$, and $\boldsymbol{\eta} = (\eta_1 \quad \eta_2 \quad \eta_3)^{\mathrm{T}}$ such as $\eta_i > |d_{5,i}|$. Substituting Eq. (26) into Eq. (25) yields

$$\dot{V}_L = -\sum_{i=1}^{3} \eta_i |\sigma_i| + \sum_{i=1}^{3} d_{5,i}\sigma_i < 0 \tag{27}$$

When the disturbance, $\boldsymbol{d}_5$ is negligible, the following setting guarantees that the finite time convergence where the finite time is within $1/k$ (s).

$$\eta_i = k|\sigma_{i\max}| \quad k > 0 \tag{28}$$

The subscript max denotes the possible maximum values of σ_i. The higher order sliding mode approach can be applied to avoid the 'chattering' phenomenon related to a sliding mode approach. The objective in this study is to check that the second order sliding surface structure is effective enough for smooth roll and pull-up coupling motions. Therefore, the following sigmoid functions are applied to achieve smooth switching, instead:

$$sigmoid(\sigma_i) = \frac{1 - e^{-\chi\sigma_i/\sigma_{i\max}}}{1 + e^{-\chi\sigma_i/\sigma_{i\max}}} \tag{29}$$

where χ is a parameter to adjust the slope around the origin of the sigmoid function. The slope around the origin equals to $\chi/2$. In this study, the slope around the origin (the trim point) corresponds to the system cut off frequency, ω_n appears in Eq. (17). The parameter, χ, can, therefore, be chosen as

$$\chi = 2\omega_n \tag{30}$$

Table 1 Simulation settings

	The chase UAV	The target aircraft
Initial Values	x_I : -2000.0 [m]	$x_{I_{TGT}}$: 200 [m]
	y_I : -2000.0 [m]	$y_{I_{TGT}}$: 0.0 [m]
	h : 524 [m]	h_{TGT} : 1524 [m]
	V : 154 [m/s]	V_{TGT} : 154 [m/s]
	ϕ : 0.0 [deg]	ϕ_{TGT} : 0.0 [deg]
Parameter values	R_d (desired distance): 200 [m]	
	ω_n : π /3[rad/s]	
	k ; 20 (1/s)	

IV. SIMULATIONS

We conducted several simulations to demonstrate the performance of the proposed integrated guidance and control system using the YF-16 model [15], whose aerodynamics is highly non-linear. One set of representative simulation results is presented in this paper. Table 1 gives the initial condition and parameter settings of these simulations. For comparison purposes, the simulation results using a conventional PPG with a dynamic inversion (DI) controller (PPG/DI) [6] are also presented. A dynamic inversion velocity controller is used to keep a desired distance from the target in both PPG/DI and SMIGC simulations. Navigation constant for the PPG is set as 2. A target aircraft is flying straight while a UAV is initially located behind the target with some offset. DI velocity controller is applied to keep the desired distance, R_d. The following assumptions were made to simplify the problem and to demonstrate the total system performance.

1) Ambient atmosphere is stationary and the earth is flat.
2) Mass of the aircraft is constant.
3) The aircraft states are available and aerodynamic uncertainties are negligible.
4) The target aircraft's position, heading, flight path, and velocity are available.

Figures 2-5 show simulation results in a scenario with chasing a straight flying target. Left Column graphs of Figs.2-5, labeled a) denote the results from using the PPG/DI whereas figures placed in the right column, labeled b) are results with the SMIGC. Figure 2 shows flight trajectories of the target and the chase UAV. Both methods can guide and control the UAV to follow the straight flying target. There is a slight difference between them at the beginning of the engagement. The UAV trajectory made with the SMIGC changes more quickly than that of the PPG/DI. The upper and the lower graphs in Fig. 3 show the time histories of the relative distance and LOS error angle (defined in Fig. 1), respectively. The relative distance between the UAV and the target gradually comes close to the predetermined desired values in both cases. (Neither method directly affects the relative distance control with the same velocity controller, which produces almost the same thrust commands in both PPG/DI and SMIGC cases. Therefore, the thrust time history is omitted in this paper.). On the other hand, the LOS error angle rapidly decreases and converges to zero with the SMIGC while the decrease is gradual in the PPG/DI case. Figures 4 and 5 show the time histories of the UAV's slow time-scale states and control surfaces' commands. Figure 4 shows the slow states of the UAV, that is, the angle of attack, roll angle, and sideslip angle. The SMIGC is able to guide the UAV toward the target aircraft direction swiftly with a proper bank and pull up coordination. Note that the sideslip history of the UAV with the SMIGC shows a larger transient response relative to that of the PPG/DI as shown in Fig. 4. The SMIGC demands more rudder inputs than the PPG/DI. Relaxing the weathercock stability of the UAV dynamics may allow for increase in its maneuverability. As can be seen in Fig. 5, the control inputs Eq. (32) with the help of the sigmoid function in Eq. (35) converge and the chattering phenomenon around the trim point often associated with sliding mode applications does not occur.

V. CONCLUSION

A sliding surface structure based on PPG and intermediate control variables of the sliding surface vector are developed for use in an IGC approach with sliding mode. The proposed sliding surface vector achieves excellent roll and pull-up motions. Performance of this technique where ***only*** 2 parameters need to be tuned was compared with the PPG/DI approach having 7-parameter tuning and the results show that the SMIGC is better in some representative simulations.

ACKNOWLEDGMENT

The first author wants to thank the National Defense Academy of Japan for giving permission for conducting guidance research at the Missouri University of Science and Technology.

REFERENCES

[1] P. Zarchan,: Tactical and Strategic Missile Guidance -Fifth Edition-, Progress in Astronautics and Aeronautic, Vol. 176, AIAA, 2002.

[2] P. Lu, D. B. Doman, and J. D. Schierman, "Adaptive Terminal Guidance for Hypervelocity Impact in Specified Direction," Journal of Guidance, Control, and Dynamics, Vol. 29, No. 2, 2006, pp. 269–278.

[3] B. S. Kim, J. G. Lee, and H. S. Han, "Biased PNG Law for Impact with Angular Constraint," IEEE Transactions on Aerospace and Electronic Systems, Vol. 34, No. 1, 1998, pp. 277–288.

[4] A. L. Smith, "Proportional Navigation with Adaptive Terminal Guidance for Aircraft Rendezvous," Journal of Guidance, Control, and Dynamics, Vol. 31, No. 6, 2008, pp. 1832–1835.

[5] R. E. Machol, W. P. Tanner, Jr, and S. N. Alexander: System Engineering Handbook, Chap. 19 Guidance, R. E. Howe, McGrow -Hill Book Company, 1965.

[6] T. Yamasaki, K. Enomoto, H. Takano, Y. Baba, and S. N. Balakrishnan, "Advanced Pure Pursuit Guidance via Sliding Mode Approach for Chase UAV," Proceedings of AIAA Guidance, Navigation and Control Conference, AIAA 2009-6298, 2009.

[7] N. Harl, and S. N. Balakrishnan, "Coordinated Rendezvous of Unmanned Air Vehicles to a Formation: A Sliding Mode Approach," Proceedings of AIAA Guidance, Navigation and Control Conference, Honolulu, Hawaii, AIAA 2008-6318, 2008.

[8] D. Galzi, and Y. Shtessel, "UAV Formations Using High Order Sliding Modes," Proceedings of the 2006 American Control Conference, Minneapolis, 2006, pp.4249-4254.

[9] T. Shima, M. Idan, and O. M. Golan, "Sliding Mode Control for Integrated Missile Autopilot-Guidance," AIAA Journal of Guidance, Control and Dynamics, Vol. 29, No. 2, 2006, pp. 250-260.

[10] I. A. Shkolnikov, and Y. B. Shtessel (2001), "Aircraft Nonminimum Phase Control in Dynamic Sliding Manifolds," AIAA Journal of Guidance, Control, and Dynamics, Vol. 24, No.3, 2001, pp. 566–572.

[11] A. Levant, "Quasi-Continuous High-Order Sliding Mode Controllers," Transactions on Aeronautical Control, Vol.50, No.11, November, 2005, pp.-1812-1816.

[12] Y. Shtessel, I. A. Shkolnikov, and A. Levant, " Guidance and Control of Missile Interceptor using Second-Order Sliding Modes," Transactions on Aerospace and Electrical Systems, Vol. 45, NO.1, January 2009, IEEE, pp. 110-124.

[13] N. Harl, S.N. Balakrishnan, and C. Phillips, "Sliding Modes Integrated Missile Guidance and Control," Proceedings of the AIAA Guidance, Navigation, and Control Conference, Toronto, Aug. AIAA 2010-7741, 2010.

[14] N. Harl, and S. N. Balakrishnan, "Reentry Terminal Guidance Through Sliding Mode Control," AIAA Journal of Guidance, Control, and Dynamics, Vol.33, No.1, 2010, pp.186-189.

[15] W. P. Gilbert, L. T. Nguyen and R. W. Van Gunst, "Simulator Study of the Effectiveness of an Automatic Control System Designed to Improve the High-Angle-of-Attack Characteristics of a Fighter Airplane," NASA TN D-8176, 1976.

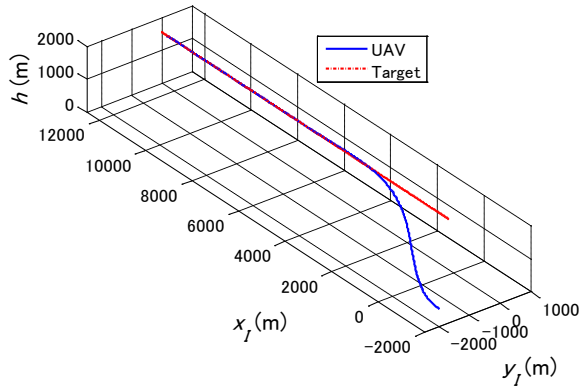

Figure 2. a)Flight path trajectories of the target and the chase UAV. (PPG/DI)

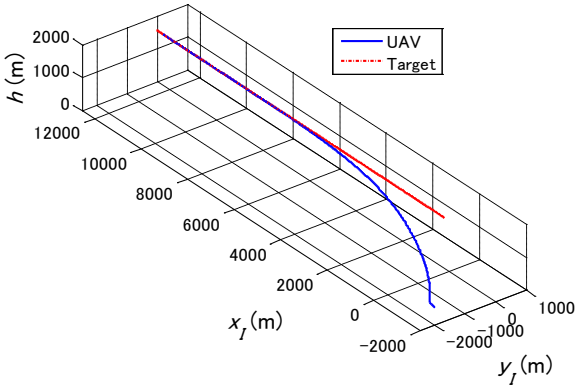

Figure 2. b)Flight path trajectories of the target and the chase UAV. (SMIGC)

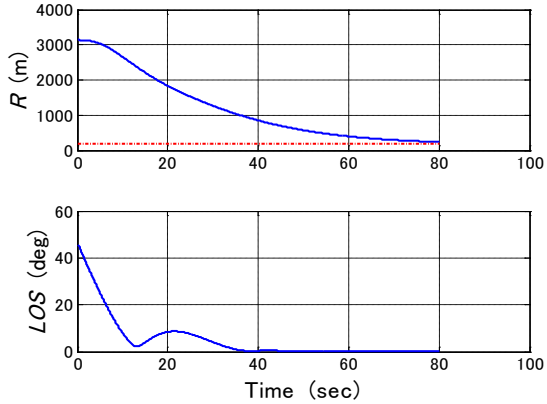

Figure 3. a) Relative distance and LOS error angle time histories. (PPG/DI)

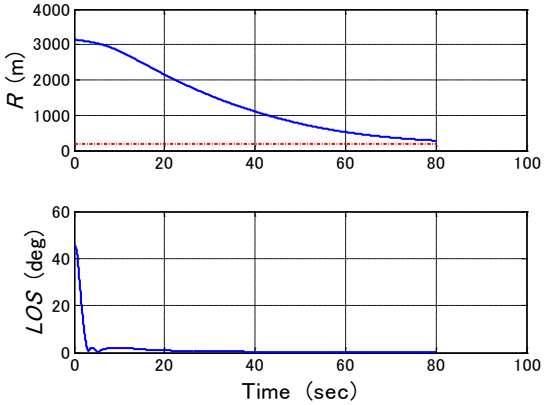

Figure 3. b) Relative distance and LOS error angle time histories. (SMIGC)

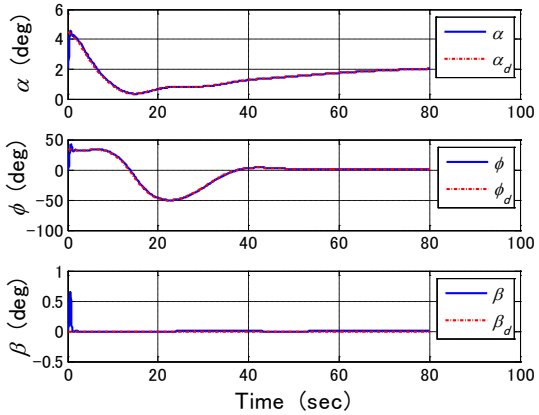

Figure 4. a) Angle of attack, roll angle, and sideslip angle time histories of the chase UAV with commanded values. (PPG/DI)

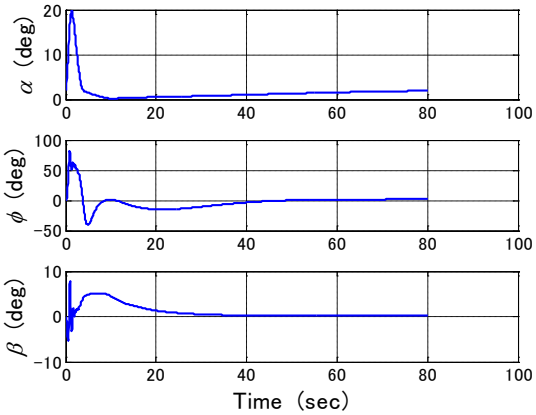

Figure 4. b) Angle of attack, roll angle, and sideslip angle time histories of the chase UAV. (SMIGC)

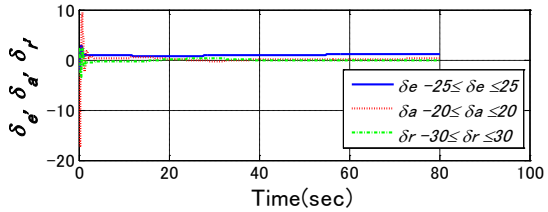

Figure 5. a) Control surfaces' command time histories. (PPG/DI)

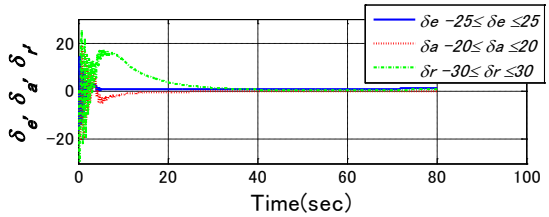

Figure 5. b) Control surfaces' command time histories. (SMIGC)